Research Article | Vol. 29, No. 20 / 27 Sep 2021 / Optics Express 32670

Optics EXPRESS

# Sub-sampled modal decomposition in few-mode fibers

**Kyuhong Choi and Changsu Jun***

*Advanced Photonics Research Institute, Gwangju Institute of Science and Technology, Gwangju 61005, Republic of Korea*
*changsu.jun@gist.ac.kr

**Abstract:** Retrieving modal contents from a multimode beam profile can provide the most detailed information of a beam. Numerical modal decomposition is a method of retrieving modal contents, and it has gained significant attention owing to its simplicity. It only requires a measured beam profile and an algorithm. Therefore, a complicated setup is not necessary. In this study, we conceived that the modal decomposition can be notably improved by data-efficiently sub-sampling the beam image instead of using full pixels of a beam profiler. By investigating the window size, the number of pixels, and algorithm for sub-sampling, the calculation time for the algorithm was faster by approximately 100 times than the case of full pixel modal decomposition. Experiments with 3-mode and 6-mode beams, which originally span 201×201 and 251×251 pixels, respectively, confirmed the remarkable improvement of calculation speed while maintaining the error function at a level of $\sim 10^{-3}$. This first demonstration of sub-sampling for modal decomposition is based on the modified stochastic parallel gradient descent algorithm. However, it can be applied to other numerical or artificial intelligence algorithms and can enhance real-time analysis or active control of beam characteristics.



## 1. Introduction

Numerical algorithms and artificial intelligence techniques have diversified the modality of beam analysis [1]. Particularly, retrieving modal weight and phase relation from a multimode beam profile has provided the most detailed information of a beam [2,3], which has become essential for applications in large-mode-area fiber-based lasers and multimode fibers [4–6]. Stochastic parallel gradient descent (SPGD) [1,3,4,7] is the most extensively studied algorithm for modal decomposition (MD). Additionally, deep learning algorithms [8–14] are frequently adopted to obtain better calculation speed or accuracy. Recently, Manuylovich et al. presented a non-iterative mathematical algorithm that did not use machine learning techniques, and the processing time was several orders of magnitude faster [15]. MD techniques continuously evolve to obtain a simple process and better performance.

Numerical modal decomposition is a technique used to find the modal weight and relative phase of each eigenmode from a measured multimode beam. For this, the SPGD algorithm reconstructs a beam by iteratively updating the coefficients of each eigenmode until the difference between the reconstructed and measured beams is within the acceptable level. Conversely, deep learning algorithms usually map the measured beam onto big data which include large amounts of pre-trained beam samples. The calculations and reconstructions are based on the whole beam image, usually measured by a beam profiler. Therefore, we propose a MD method based on selected pixels of the beam image instead of using full pixels. Each fiber eigenmode has a specific intensity at a specific position, and a measured multimode beam is a combination of each eigenmode. Therefore, a pixel of the measured beam should include the information of all the constituting eigenmodes. This makes a system of equations. $N$-mode beam comprises variables of $N$ modal weight and $N$-1 relative phase coefficients. Therefore, a system of at least $2N$-1 equations can provide solutions, indicating that at least $2N$-1 pixels are sufficient

#438533 https://doi.org/10.1364/OE.438533
Journal © 2021 Received 22 Jul 2021; revised 13 Sep 2021; accepted 13 Sep 2021; published 24 Sep 2021

to solve the coefficients of each eigenmode. Initially, we investigated the feasibility of the sub-sampled MD with approximately 2$N$-1 pixels and observed that the selected pixels were not independent of each other or effective enough, resulting in non-correspondence to the full pixel MD. Therefore, we investigated the window size for sub-sampling the beam, the minimum number of pixels, and the algorithm required to fulfill the sufficient condition for sub-sampled MD, which will significantly decrease the computational cost. Previously, the sub-sampling technique for data-efficient calculation was adopted in diverse image processing applications such as ptychography or magnetic resonance imaging, which can be implemented in spatial or Fourier domains [16–20]. The embodiment of sub-sampling included the procedures of sampling, filtering, and weighting, while all the studies provided reduced calculation times and high-quality results compared to the full implementation [16–20]. Sub-sampling for MD of laser beams has not been demonstrated beforehand, and it is slightly different from the aforementioned image processing studies. The fiber eigenmodes as a basis for decomposition are known in advance. Therefore, the number of required pixels after optimization can be smaller.

In this study, we demonstrate the sub-sampled modal decomposition of laser beams based on modified stochastic parallel gradient descent algorithm. Utilization of only 2$N$-1 pixels for MD was first verified through simulation to obtain an insight into the feasibility of the sub-sampled MD, followed by the optimization of window size, the number of pixels, and algorithm for sub-sampling to satisfy the conditions of accuracy and speed enhancement. Additionally, the SPGD algorithm was modified to address local minima [7] and real-beam issues such as beam center or beam size mismatch and the noises caused by imperfect experimental conditions [21,22]. Real-beam MD, and simulation with noisy beams, reveal that discriminating global minimum is difficult and the error function cannot be lower than $\sim 10^{-4}$. A compromised approach is obtaining the solution from the smallest error function after finding several convergences. The reduction in the number of pixels to 5×5 from 201×201, and to 7×7 from 251×251, in 3-mode and 6-mode beams, respectively, resulted in remarkable improvement of calculation speed by two orders of magnitude, while maintaining the high accuracy of error function at a level of $\sim 10^{-3}$, which is comparable to the case of full pixel MD of real beams.

## 2. Sub-sampled modal decomposition based on modified SPGD algorithm

The electric field $U$ from a multimode optical fiber can be represented as a linear superposition of eigenmodes,

$$U(x,y) = \sum_{j=1}^{N} \rho_j e^{i\phi_j} \psi_j(x,y) \tag{1}$$

where $N$ is the number of guided modes, $\rho^2$ and $\phi$ are the modal weight and phase of the $j$th mode, respectively, and $\psi(x,y)$ is the normalized amplitude of each linearly-polarized (LP) mode. In the SPGD algorithm for MD, a beam intensity distribution $I(x,y) = |U(x,y)|^2$ is reconstructed with random modal coefficients and is compared with the measured beam. The iteration of reconstruction continues by updating the modal coefficients according to the algorithm until the shape similarity between the reconstructed and measured beams falls within an acceptable level. For the shape comparison, an error (cost or merit) function $D$ is usually defined as,

$$D = 1 - \frac{\iint I_{me}(x,y) I_{re}(x,y) dxdy}{\sqrt{\iint I_{me}^2(x,y)dxdy \iint I_{re}^2(x,y)dxdy}} \tag{2}$$

where $I_{me}(x,y)$ is the measured beam intensity, and $I_{re}(x,y)$ is the reconstructed beam intensity. $D$ is a value between 0 and 1, which is 0 when the reconstructed beam is identical to the measured beam, in the case of perfect MD. This definition was more accurate and consistent for the various pixel sizes in this work over the residual intensity and other definitions.

Optics EXPRESS

Conventional SPGD algorithm calculates the value of $D$ twice in an iteration to find the smaller of the +/- perturbations. Therefore, the computational cost is greater as the number of pixels of a measured beam increases to 201×201 or 251×251. The sub-sampled MD, thus, will significantly enhance the calculation time by reducing the number of required pixels. However, it requires a comparable result with the case of full pixel MD. The error function for sub-sampled MD can then be defined as,

$$D_{sub} = 1 - \frac{\sum_{i=1}^{N_p} I_{me}(x_i, y_i) I_{re}(x_i, y_i)}{\sqrt{\sum_{i=1}^{N_p} I_{me}^2(x_i, y_i)\ \sum_{i=1}^{N_p} I_{re}^2(x_i, y_i)}} \tag{3}$$

where $i$ and $N_p$ are the index and the total number of selected pixels.

As stated in the introduction, the modal coefficients acquired from $N$-mode beams include $N$ modal weight, $\{\rho_j | \, j = 1, 2, \ldots, N\}$ and $N$-1 relative phase coefficients, $\{\varphi_j = \phi_j - \phi_1 | \, j = 2, 3, \ldots, N\}$. Therefore, ideally, a system of 2$N$-1 equations, or 2$N$-1 pixels is sufficient to solve the coefficients of each eigenmode as depicted in Figs. 1(a) and 1(b). To study the feasibility of the sub-sampled MD with approximately 2$N$-1 pixels, simulation of 4-, 5- and 6-pixel MDs for noiseless 3-mode beams was performed as shown in Fig. 1(c). Initially, the error functions of sub-sampled MD, $D_{sub}$ for 10 different random beams and 50 repetitions each, were calculated. Revealing the modal contents of random beams is meaningless in this work and thus they are not described. By limiting the iteration parameter, we obtained a wide range of $D_{sub}$ values to verify the linearity between the two results of sub-sampled and full pixel error functions. The modal coefficients acquired by sub-sampled MD were thereafter applied to the other pixels and the error functions of full pixels, $D_{regen}$ were regenerated. If the modal coefficient solutions determined using few-pixel MD can be utilized for other pixels, it can be assumed that the $D_{regen}$ values are linearly proportional to the corresponding $D_{sub}$ values. If linearity is not ensured, it implies the modal coefficient solutions are different depending on the selected pixels, and the sub-sampling MD does not function properly. As a reference, the black dashed diagonal in Fig. 1(c) represents the cases of identical solutions between the sub-sampled and full-pixel error functions. The result of 4-pixel MD (black square dot) in Fig. 1(c) does not exhibit linearity between $D_{regen}$ and $D_{sub}$, while that of 5-pixel MD (red circle dot) begins to show linearity depending on the samples. The result of 6-pixel MD shows improved linearity although it has offset from the diagonal line owing to the errors of the acquired modal contents. Similarly, 10-, 11- and 12-pixel MDs for 6-mode beams were performed as seen in Fig. 1(d). The 11-pixel MD, which corresponds to the case of 2$N$-1 pixels of $N$-mode beam, shows linearity depending on samples and the linear tendency is improved in 12-pixel MD. The distribution of results is more scattered in 6-mode beams than that of 3-mode beams owing to the complicated beam shape. The result of Fig. 1 implies that sub-sampled MD with 2$N$-1 pixels for $N$-mode beam is possible. However, linear dependence between pixels can result in an underdetermined system of equations, and the linear independence between pixels in a beam can be diminished in other beam shapes. Therefore, the selection of 2$N$-1 pixels is crucial.

For obtaining universal sub-sampled MD and addressing noisy measured beams, the number of required pixels should be greater than 2$N$-1, while the sampling pattern should be simple to ensure a short calculation time. Therefore, we investigated the window size for sub-sampling the beam, the minimum number of pixels, and the algorithm to fulfill the sufficient condition for sub-sampled MD.

Figure 2 demonstrates the procedure of the modified SPGD algorithm. The basic flow is similar to that of the conventional SPGD algorithm. However, it is modified to include the process of sub-sampling the beam profile and eigenmodes. Additionally, this procedure addresses local minima [7] and real-beam issues such as noise caused due to imperfect experiment conditions [21,22]. The previous simulation algorithm proposed by our group called enhanced SPGD algorithm [7], applies large perturbations whenever local minima are observed. This feature

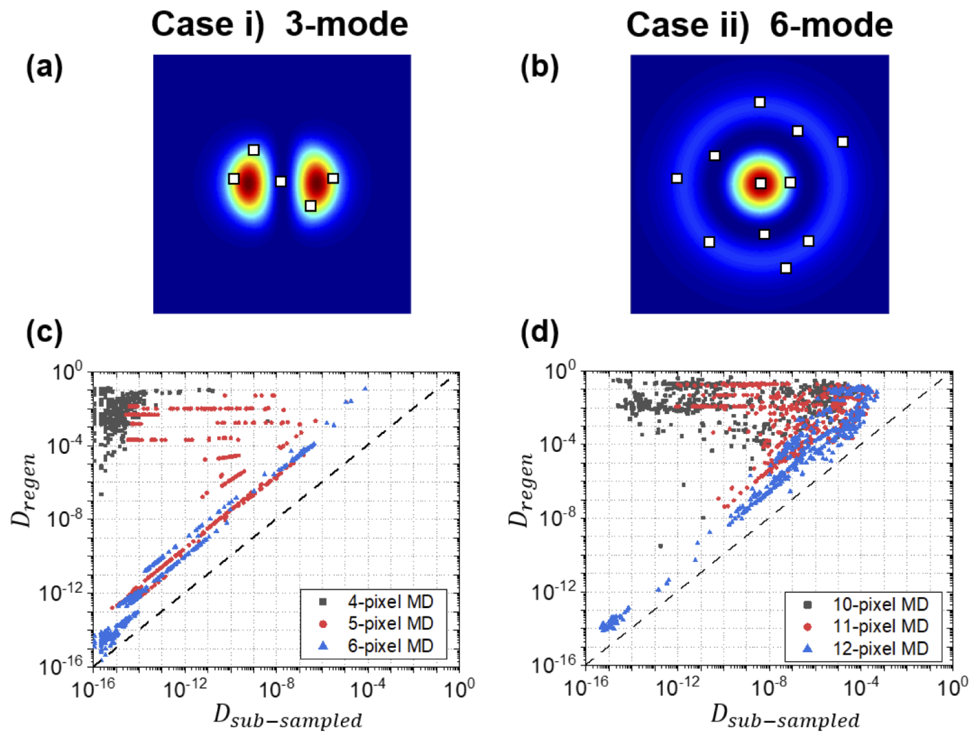


**Fig. 1.** Schematic images of ideal sub-sampled MD for (a) 3-mode and (b) 6-mode beams, respectively. The relations between sub-sampled and full pixel error functions are displayed for (c) 3-mode and (d) 6-mode beams, respectively.

was included in the modified SPGD algorithm shown in Fig. 2. The algorithm repeats iterations until the error function reaches the target value. However, this method is not successful and needs to be revised in case of noisy real beams. Real beam MD and simulations conducted with noisy beams reveal that reaching the target error function or discriminating global minimum is challenging. Therefore, the error function cannot be lower than $\sim 10^{-4}$, as reported in previous researches [4,5,9,12,21]. A compromised approach is selecting the optimum error function after obtaining several convergences or local minima during iterations. To satisfy the conditions of calculation speed and accuracy, the number of convergences to find during iterations should be optimized as well.

Determining the sample pattern is an issue while optimizing the number of required pixels of sub-sampled MD. From the result of Fig. 1, the criticality of selecting special pixels was preempted, possibly provoking additional complications instead of taking advantage of the sub-sampling process. Instead, a simple and periodic two-dimensional sampling pattern such as a square pattern, is preferred to maximize the advantage of sub-sampling. Meanwhile, the window size for sub-sampling should be considered as well. It should be noted that relevant beam intensities of $N$-mode beams are within the boundary of the highest mode, while the surrounding region of the beam profile has a significantly low intensity, considered as noise. Limiting the window size will also reduce the number of required pixels, compared with that of spanning the sampling pattern on the whole plane of the charged-coupled device (CCD). The white circles of the inset images in Figs. 3(a) and 3(b) are the references that denote the envelope of the highest modes, $LP_{11}$ and $LP_{02}$ in 3-mode and 6-mode beams, respectively. In this study, the envelope of each mode was defined as the perimeter in which the fraction of optical power drops to ~86.5%

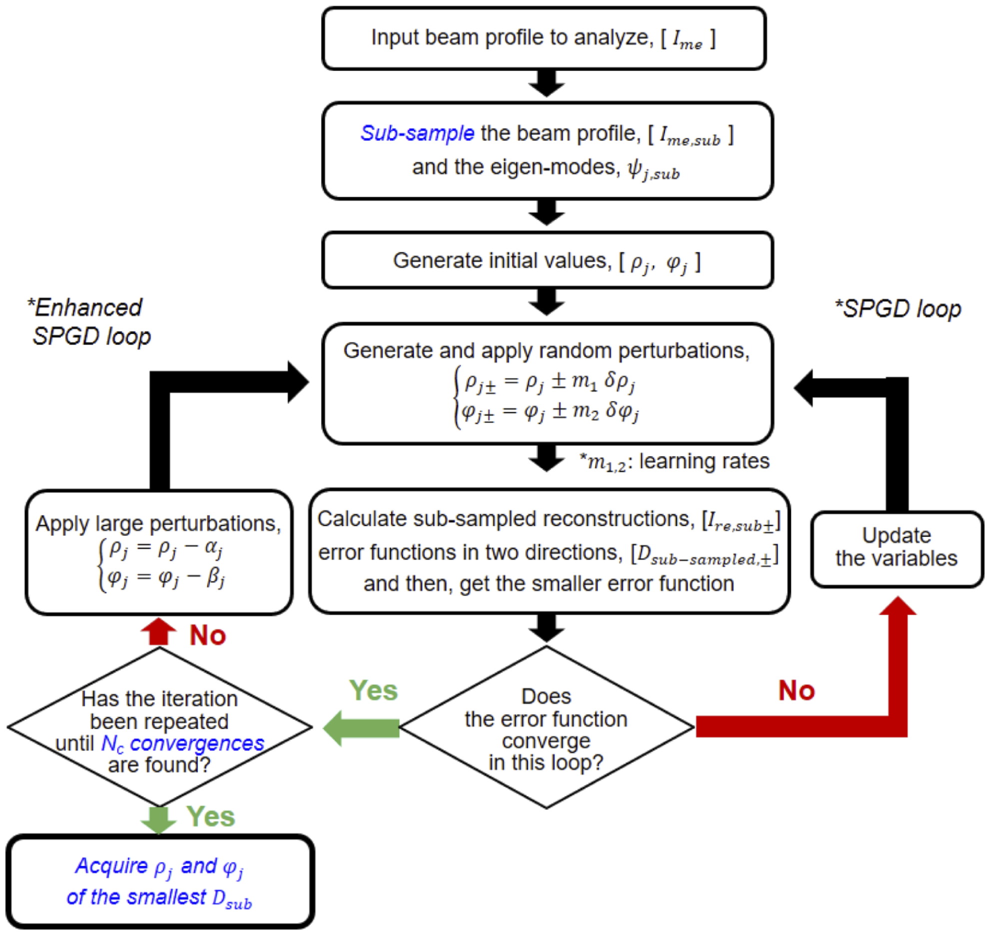


**Fig. 2.** Modified SPGD algorithm

of the total power. After determining the square-patterned sampling around the boundary of the highest mode, a detailed window size was examined (Fig. 3). The X-axis values represent the relative distance between pixels normalized by that of the inscribed square, corresponding to 1.0. In Fig. 3, 100 random beams with 35 dB signal-to-noise ratio (SNR) and 30 repetitions each were calculated for MD, and the averaged $D_{regen}$ was set as the Y-axis value for each window size. Like the case of Fig. 1, revealing the modal contents of 100 random beams is meaningless and thus they are not described. The SNR in the simulation was determined after analyzing that of the real beams in the spatial Fourier domain [21,22]. In Fig. 3(a) for 3-mode beams, $D_{regen}$ showed low values and negligible difference in the range of 0.5–1.5. Values below 0.4 and above 2.0 contained huge errors. In the case of 6-mode beams shown in Fig. 3(b), a value in the range of 0.9–1.6 can be used for sub-sampling. The examples in Fig. 3 are based on 5×5 and 7×7 pixels, respectively, and other cases with M×M pixels had also approximately 1.0 in common within the plateau region in which $D_{regen}$ showed low values and negligible difference. Too small or too large windows compared to the beam size increase the chances of linear dependence between pixels or local minimum by losing many relevant pixels, and thus the errors are increased. Therefore, we determined the window size for sub-sampling as the inscribed square region within the envelope of the highest mode as seen in the insets of Fig. 3. This constraint utilizes high SNR pixels in the central region, and reduces the number of required pixels as explained further.

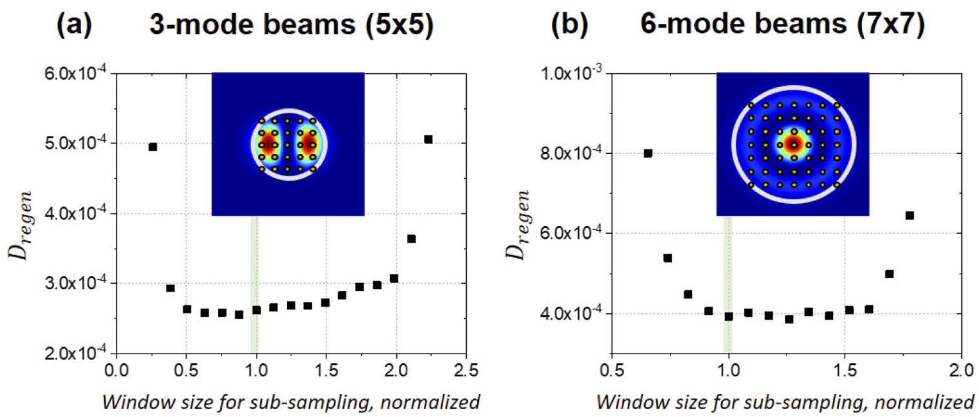


**Fig. 3.** Optimization of the window size for sub-sampling in (a) 3-mode and (b) 6-mode beams with 35 dB SNR. The X-axis with 1.0 (light green line) corresponds to the case of the inscribed square within the white circle, and the other values represent the relative distance between pixels normalized by the inscribed square.

After determining the square sampling pattern, the number of required pixels for sub-sampling was examined. Figure 4 shows the linearity results between $D_{regen}$ and $D_{sub}$, as indicated in Fig. 1, obtained by changing the number of pixels, M×M, for sub-sampling. In this simulation, 100 beams and 30 repetitions were calculated for MD. As a reminder that the modal coefficients acquired by sub-sampled MD were applied to other pixels, and the error functions of full pixel MD, $D_{regen,}$ were regenerated. If the modal coefficient solutions determined using few-pixel MD can be utilized for other pixels, it can be assumed that the $D_{regen}$ values are linearly proportional to the corresponding $D_{sub}$ values. Four cases were investigated, 3-mode beams without noise (Fig. 4(a)) and with 35 dB SNR (Fig. 4(b)), and 6-mode beams without noise (Fig. 4(c)) and with 35 dB SNR (Fig. 4(d)). For each case, full pixel MD was first calculated as a reference (black square dot), 201 ×201 in Figs. 4(a) and 4(b), and 251 ×251 in Fig. 4(c) and 4(d), respectively, and the results were placed on the diagonal.

The smallest 2-D array of pixels in a square is 3 ×3 and the result in Fig. 4(a) (red circle dot) is linear, but it is scattered within a certain offset from the diagonal. This implies that the modal contents solutions acquired from 3 ×3 pixels result in increased errors. Hence, higher values of $D_{regen}$ are obtained than that of $D_{sub}$ when applied to all pixels. Therefore, the number of pixels should be increased. However, the linearity and noise were notably improved from 5 ×5 pixels (blue triangle dot, green inverted triangle dot, and violet diamond dot). The MD of noisy beams was simulated to mimic real beams, as seen in Fig. 4(b). The overall tendency was the same as Fig. 4(a), but $D_{regen}$ did not reduce to less than approximately $2{\times}10^{-4}$, while $D_{sub}$ could span down to $\sim10^{-5}$. The reason for this nonlinearity is because sub-sampling to limited pixels in a noisy beam has the probability of attaining low noise pixels depending on the beam shapes or applied random noise. Subsequently. $D_{sub}$ can be small. However, after the full pixel application or $D_{regen}$ in a noisy beam, the level of noise is averaged out, resulting in a higher value of $D_{regen}$. Therefore, noisy beam has a certain limit of $D_{regen}$, and it will depend on the SNR of a beam. Additionally, a smaller number of pixels, for example, 3 ×3, has a greater probability of obtaining low noise pixels. Therefore, this results in lower $D_{sub}$ than that of the case of a higher number of pixels, as seen in the vicinity of $\sim10^{-5}$ of Fig. 4(b). Based on the result of Fig. 4(b), 5 ×5 pixels were selected for sub-sampled MD in 3-mode real beams. Similarly, 6-mode beams without noise, and with noise were investigated as seen in Figs. 4(c) and 4(d), respectively. 3 ×3 pixels in 6-mode beams are below $2N$-1 pixels of $N$-mode beams.

Optics EXPRESS

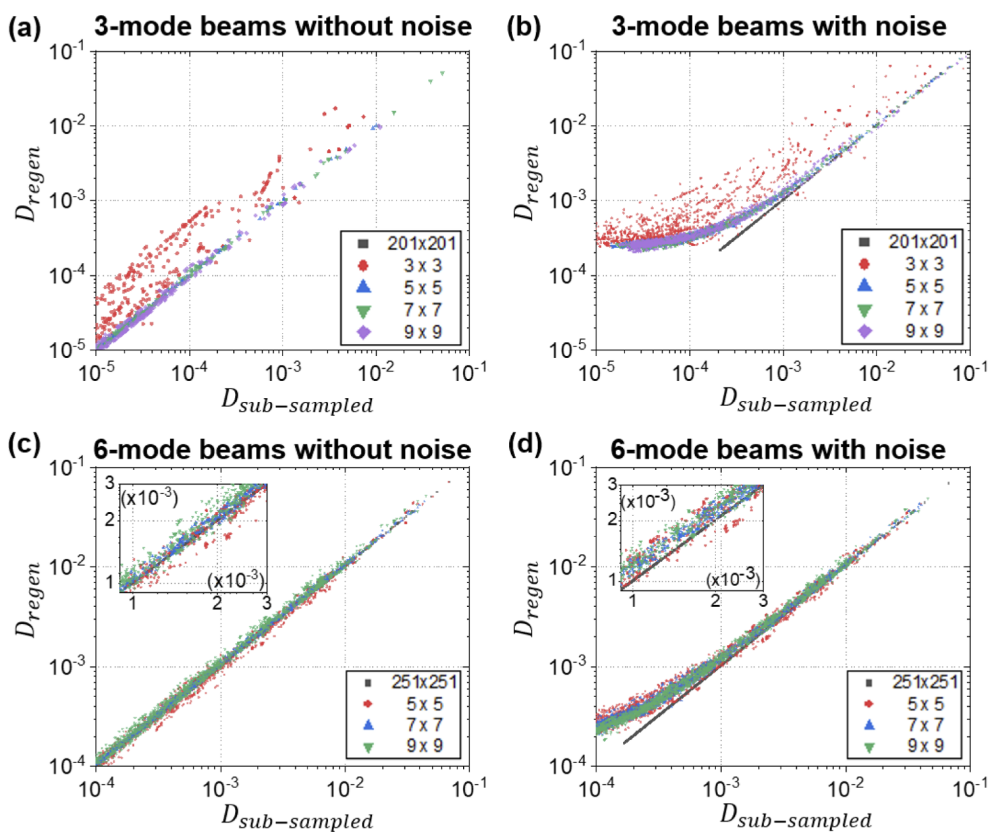


**Fig. 4.** Optimization of the number of pixels for sub-sampling in 3-mode beams (a) without noise and (b) with noise, and in 6-mode beams (c) without noise and (d) with noise.

Hence, they are omitted. In 6-mode beams, the tested pixel arrays (red circle dot, blue triangle dot, green inverted triangle dot) exhibited appropriate linearities and errors although a smaller number of pixels had a slightly broader distribution of dots and poor noise characteristics as seen in the inset of Figs. 4(c) and 4(d). The saturation of $D_{regen}$ is also observed for noisy beams in the vicinity of $\sim 10^{-4}$ of Fig. 4(d). 7 ×7 pixels were determined for sub-sampled MD in the case of 6-mode real beams to obtain an improved accuracy.

The last factor to be determined is the number of convergences during the iteration of the algorithm as displayed in Fig. 5 and Fig. 6.

As mentioned in the introduction, real beam MD cannot obtain an error function lower than $\sim 10^{-4}$. In simulation studies, the error function obtained can be $\sim 10^{-7}$ [7] because every beam is in a perfect shape without noise. However, in a real beam analysis, several factors such as beam size mismatch, beam center mismatch, and SNR of the images [21,22], degrade the error function to approximately $10^{-3}$. Therefore, as shown in Fig. 2, the SPGD algorithm should be modified to address the real beam issues. The modified algorithm finds convergence of the error function during iterations and repeats it $N_c$ times to check the possibility of a better error function, and the minimum value is considered as the final error function. Here, the target error function was additionally set as $10^{-3}$ for improved accuracy and then the data below the target value could continue to iterate. The number of convergences to determine during iterations was optimized to satisfy the conditions of calculation speed and accuracy in 3-mode and 6-mode beams. Figures 5(a) and 5(b) are the error functions and the errors in 3-mode

Optics EXPRESS

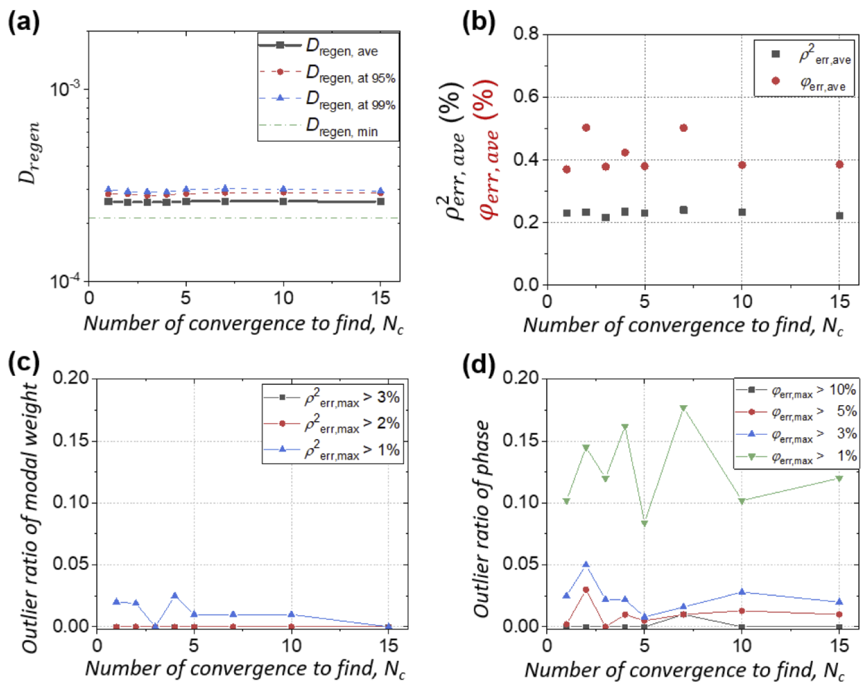


**Fig. 5.** Simulation results of 3-mode beams depending on the number of convergences to be determined during the iteration of the algorithm. (a) The error functions, (b) averaged errors of modal weight and phase, outlier ratio of (c) modal weight and (d) phase. $\rho^2_{err,\ ave}$ and $\varphi_{err,\ ave}$ are the averaged errors of modal weight and relative phase, respectively.

beams, as the function of the number of convergences to find, $N_c$, and Figs. 5(c) and 5(d) are the outlier ratios of modal weight and phase respectively depending on the maximum errors of modal weight and phase. Here, the percentage errors of modal weight and phase are calculated as, $\rho^2_{\mathrm{err},j} = (\rho^2_{re,j} - \rho^2_{gen,j}) \times 100$, $\varphi_{\mathrm{err},j} = (\varphi_{re,j} - \varphi_{gen,j})/\pi \times 100$, where the subscript *re* denotes reconstructed beam and *gen* generated beam. In Fig. 5(b), the average values are displayed. $D_{regen,\ ave}$ in Fig. 5(a) is the averaged error function to observe the overall behavior, $D_{regen,\ at\ 95\%}$ and $D_{regen,\ at\ 99\%}$ are the error functions at 95% and 99%, respectively, from the best value to obtain an insight about the error functions if the worst 5% or 1% is neglected, respectively, and $D_{regen,\ min}$ is the minimum error function to verify the lower bound. To obtain the statistics, 100 beams and 30 repetitions were calculated. The averaged error function, $D_{regen,\ ave}$, $D_{regen,\ at\ 95\%}$ and even $D_{regen,\ at\ 99\%}$ for 3-mode beams in Fig. 5(a) show consistent results regardless of $N_c$. The calculation time was linearly proportional within the range of 0.028 ~ 0.210 seconds to the number of convergence although it is not displayed. MD for 3-mode beams did not have a local minimum because of the simple composition. Therefore, one convergence during iteration was sufficient to obtain the fastest calculation time. The averaged errors of modal weight and relative phase were below 0.3% and 0.5%, respectively, as seen in Fig. 5(b). Figures 5(c) and 5(d) are the outlier ratios of modal weight and phase respectively depending on the maximum errors of modal weight and phase. If we define the error criteria as 5%, the outliers of modal weight and phase are nearly 0% and below 2.5%, respectively. In 6-mode beams, the result is worse than that of 3-mode beams because of the complex composition and local minima as observed in Fig. 6. Figures 6(a) and 6(b) are the error functions and the errors in 6-mode beams. As the number of convergences to determine during iteration increases up to 15 times, the error functions and the errors approach minimum values, while the calculation time increases within

Optics EXPRESS

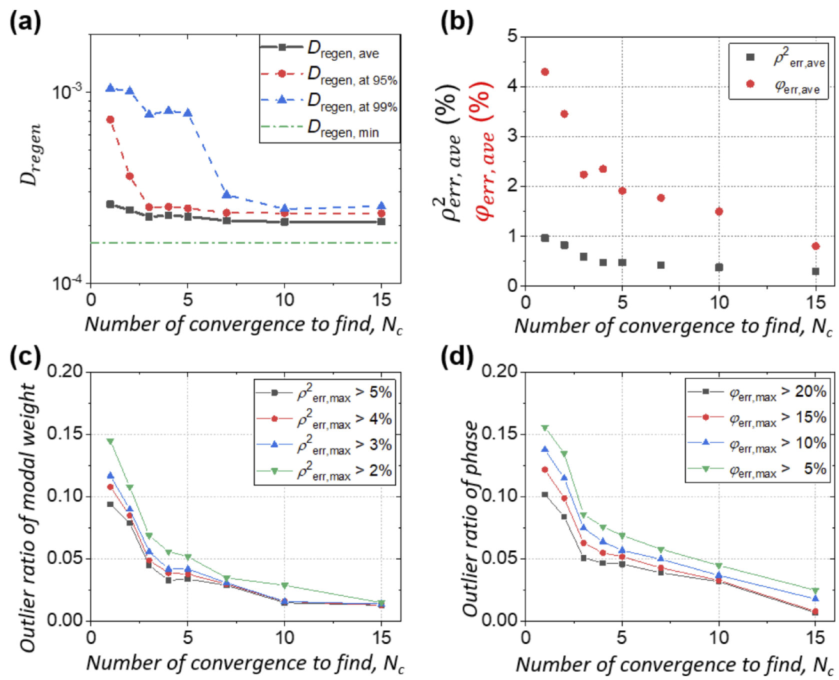


**Fig. 6.** Simulation results of 6-mode beams depending on the number of convergences. (a) The error functions, (b) averaged errors of modal weight and phase, outlier ratio of (c) modal weight and (d) phase.

0.064 ~ 0.519 seconds. The selection of the number of convergences depends on the weight between calculation time and accuracy. $N_c$ = 5 was selected for 6-mode beams based on the result that the averaged errors are below 2% and the outliers of modal weight and phase are below 5% and 7%, respectively, as seen in Fig. 6(b)–6(d).

## 3. Sub-sampled MD of real beams

After simulating the conditions of the window size, the number of pixels, and algorithm for data-efficient and time-efficient calculation, sub-sampled MD was applied to real beams.

The experimental setup for the measurement of 3-mode and 6-mode beams is shown in Fig. 7. A 1064-nm polarization-maintaining laser diode was used as a light source. The 3-mode fiber had a core diameter of 20 µm and a numerical aperture (NA) of 0.06, while 6-mode fiber had a core diameter of 25 µm and a NA of 0.065. After the beam was collimated by L1, it was coupled into the few-mode fiber (FMF) through L2, and the misalignment between L2 and FMF by a 3-axis stage induced higher-order modes. The residual cladding modes induced additional artifacts in the final beam image. Therefore, a high-index gel was used to remove them. The outgoing beam from the FMF was expanded by 20 times using L3 and L4, and the final near field image was captured by a CCD camera. The half-wave plate was used to align the light polarization with the PM fiber axis, and the polarizer was used to measure the output polarization state. Various multimode beams were excited by adjusting the misalignment at the fiber input.

Figure 8 is the result of sub-sampled MD for 3-mode and 6-mode real beams, which is compared with the result of all-pixel MD. The first row represents the measured beams, two 3-mode, and four 6-mode beams, and the second row represents the result of conventional all-pixel MD. The number of pixels are 201 ×201 in 3-mode beams, and 251 ×251 in 6-mode beams, which are the same as the simulations. The error functions $D$ of the all-pixel MD were

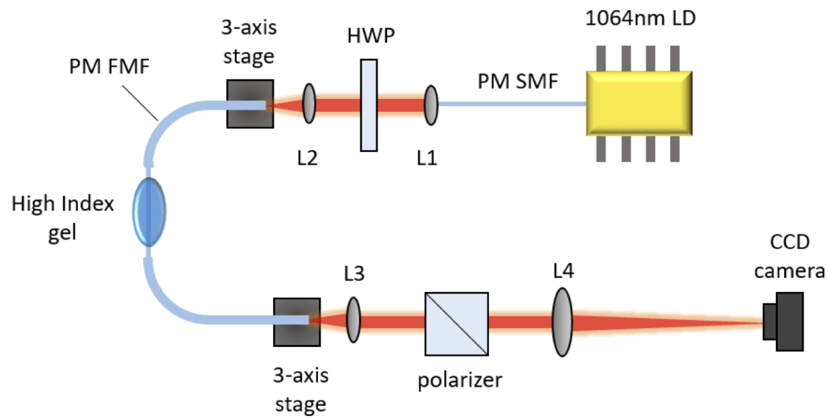


**Fig. 7.** The experimental setup for 3-mode and 6-mode beams measurement. LD: laser diode, PM: polarization-maintaining, SMF: single-mode fiber, L1, 2, 3, 4: Lens, HWP: half-wave plate, FMF: few-mode fiber.

of order of $\sim 10^{-3}$, and the calculation times were up to 14.2 seconds, as denoted in the figures. Conversely, sub-sampled MD for 3-mode beams used 5 ×5 square-patterned pixels as examined using noisy beams in Figs. 3–4, and 7 ×7 pixels in the case of 6-mode beams. According to the results of Figs. 5 and 6 for both MDs, $N_c$ = 1 and $N_c$ = 5 were set for 3-mode and 6-mode beams, respectively. To assess the repeatability, sub-sampled MD was repeated 100 times for each beam and then the maximum values among the standard deviation of each modal content were summarized at the bottom of Fig. 8. The beam shape similarity was indistinguishable among the measured, all-pixel MD and sub-sampled MD, and there was a negligible difference of error functions between all-pixel and sub-sampled MDs. Notably, the calculation time of sub-sampled MD was faster by ~100 times than that of all-pixel MD, while maintaining the accuracy. This work was based on the modified stochastic parallel gradient descent algorithm but

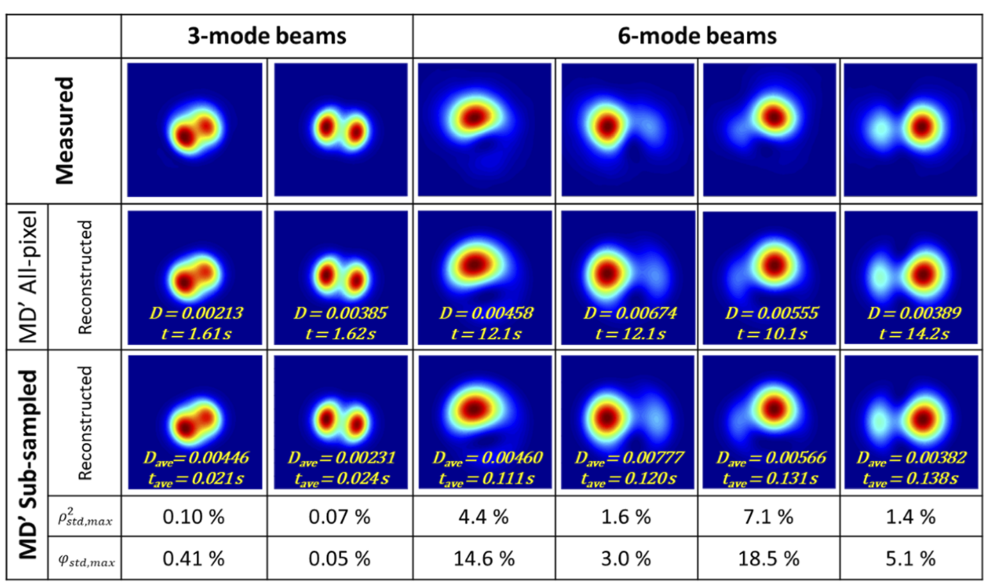


**Fig. 8.** Result of sub-sampled MD of real beams

Optics EXPRESS

presents high accuracy and speed without complicated deep learning algorithms. The scheme of sub-sampling can also be applied while optimizing the beam size mismatch and beam center mismatch [21,22] in the first setup of real beam MD.

The demonstrated sub-sampled MD in this work utilizes only a near field image, and can be used to retrieve the modal weight of each mode faster in the analysis of modal instability of high power fiber laser or mode division multiplexed optical communication. Sub-sampled MD based on a pair of near field and far field images or multiple plane images can provide the most detailed modal contents with high accuracy and speed in future studies. In this work, 3-mode and 6-mode fibers were used in simulation and experiment. However, the sub-sampling technique can surely be applied to multimode beams with a higher number of modes. In Fig. 3, the window size for sub-sampling was determined as the inscribed square region within the envelope of the highest mode. The same criterion can be applied to the beams with a higher number of modes because the boundary includes most of the effective pixels within. Next, the number of required pixels within the window size can be considered as a spatial resolution for sub-sampling. Therefore, the complexity of each higher-order mode may determine the required number of pixels. As the number of modes increases, more pixels will be required, but they are not linearly proportional. According to the simulation study in 8-mode and 10-mode beams (100 beams and 30 repetitions each, 35 dB SNR), 7×7 pixels were enough for sub-sampled MD although the results are not displayed.

## 4. Conclusion

Sub-sampling is a method used in the field of image processing. In this study, sub-sampling was conceived to be applied to modal decomposition of complicated laser beams. A feature of sub-sampled MD in few-mode fibers is that the fiber eigenmodes are known in advance. Therefore, the number of required pixels can be smaller than that of the conventional image processing. By investigating the window size, the number of pixels, and algorithm for sub-sampling, conditions for data-efficient sub-sampled MD could be acquired in 3-mode and 6-mode beams. Experiments of sub-sampled MD with 3-mode and 6-mode beams, which originally spanned 201×201 and 251×251 pixels, respectively, reduced the number of required pixels to 5×5 and 7×7, respectively. This resulted in a remarkable improvement of calculation speed (two orders of magnitude) while maintaining the high accuracy of the error function at a level of $\sim 10^{-3}$, which is comparable to the case of full pixel MD of real beams. This demonstration was based on the modified stochastic parallel gradient descent algorithm. However, it presented high accuracy and speed without complicated deep learning algorithms. The concept of sub-sampled MD can be applied to other numerical or artificial intelligence algorithms, and it can enhance real-time analysis and provide active control of beam characteristics.

**Funding.** Gwangju Institute of Science and Technology (K13720).

**Disclosures.** The authors declare no conflicts of interest.

**Data availability.** Data underlying the results presented in this paper are not publicly available at this time but may be obtained from the authors upon reasonable request.

### References

1. Y. An, J. Li, L. Huang, L. Li, J. Leng, L. Yang, and P. Zhou, "Numerical mode decomposition for multimode fiber: From multi-variable optimization to deep learning," Opt. Fiber Technol. **52**, 101960 (2019).
2. R. Brüning, P. Gelszinnis, C. Schulze, D. Flamm, and M. Duparré, "Comparative analysis of numerical methods for the mode analysis of laser beams," Appl. Opt. **52**(32), 7769 (2013).
3. H. Lü, P. Zhou, X. Wang, and Z. Jiang, "Fast and accurate modal decomposition of multimode fiber based on stochastic parallel gradient descent algorithm," Appl. Opt. **52**(12), 2905 (2013).
4. L. Huang, S. Guo, J. Leng, H. Lü, P. Zhou, and X. Cheng, "Real-time mode decomposition for few-mode fiber based on numerical method," Opt. Express **23**(4), 4620 (2015).
5. L. Huang, T. Yao, J. Leng, S. Guo, R. Tao, P. Zhou, and X. Cheng, "Mode instability dynamics in high-power low-numerical-aperture step-index fiber amplifier," Appl. Opt. **56**(19), 5412 (2017).

Optics EXPRESS


6. Z. Zhang, C. Guo, L. Cui, Q. Mo, N. Zhao, C. Du, X. Li, and G. Li, "21 Spatial mode erbium-doped fiber amplifier for mode division multiplexing transmission," Opt. Lett. **43**(7), 1550 (2018).
7. K. Choi and C. Jun, "High-precision modal decomposition of laser beams based on globally optimized SPGD algorithm," IEEE Photonics J. **11**(5), 1–10 (2019).
8. L. Li, J. Leng, P. Zhou, and J. Chen, "Multimode fiber modal decomposition based on hybrid genetic global optimization algorithm," Opt. Express **25**(17), 19680 (2017).
9. Y. An, L. Huang, J. Li, J. Leng, L. Yang, and P. Zhou, "Learning to decompose the modes in few-mode fibers with deep convolutional neural network," Opt. Express **27**(7), 10127 (2019).
10. H. Gao, H. Hu, Y. Zhao, and J. Li, "A real-time fiber mode demodulation method enhanced by convolution neural network," Opt. Fiber Technol. **50**, 139–144 (2019).
11. S. Rothe, Q. Zhang, N. Koukourakis, and J. W. Czarske, "Deep learning for computational mode decomposition in optical fibers," Appl. Sci. **10**(4), 1367 (2020).
12. Y. An, L. Huang, J. Li, J. Leng, L. Yang, and P. Zhou, "Deep learning-based real-time mode decomposition for multimode fibers," IEEE J. Sel. Top. Quantum Electron. **26**(4), 1–6 (2020).
13. X. Fan, F. Ren, Y. Xie, Y. Zhang, J. Niu, J. Zhang, and J. Wang, "Mitigating ambiguity by deep-learning-based modal decomposition method," Opt. Commun. **471**, 125845 (2020).
14. S. Rothe, Q. Zhang, N. Koukourakis, and J. Czarske, "Intensity-only mode decomposition on multimode fibers using a densely connected convolutional network," J. Lightwave Technol. **39**(6), 1672–1679 (2021).
15. E. S. Manuylovich, V. V. Dvoyrin, and S. K. Turitsyn, "Fast mode decomposition in few-mode fibers," Nat. Commun. **11**(1), 5507 (2020).
16. F. Banterle, M. Corsini, P. Cignoni, and R. Scopigno, "A low-memory, straightforward and fast bilateral filter through subsampling in spatial domain," Comput. Graph. Forum **31**(1), 19–32 (2012).
17. S. Dong, Z. Bian, R. Shiradkar, and G. Zheng, "Sparsely sampled Fourier ptychography," Opt. Express **22**(5), 5455 (2014).
18. A. Levina and V. Priesemann, "Subsampling scaling," Nat. Commun. **8**(1), 15140 (2017).
19. A. Stevens, H. Yang, W. Hao, L. Jones, C. Ophus, P. D. Nellist, and N. D. Browning, "Subsampled STEM-ptychography," Appl. Phys. Lett. **113**(3), 033104 (2018).
20. C. D. Bahadir, A. Q. Wang, A. V. Dalca, and M. R. Sabuncu, "Deep-learning-based optimization of the under-sampling pattern in MRI," IEEE Trans. Comput. Imaging **6**, 1139–1152 (2020).
21. K. Choi, Y. Kim, Y. Yun, Y.-C. Noh, and C. Jun, "Study on factors degrading the accuracy of real beam modal decomposition," Curr. Opt. Photonics **5**(2), 93–100 (2021).
22. K. Singh, P. Sharma, A. Suchita, B. Dixit, R. D. Srinivasan, D. Koilpillai, and Venkitesh, "Theoretical and experimental investigation of the sources of error in stochastic parallel gradient descent-based digital modal decomposition technique," OSA Continuum **4**(7), 1916–1932 (2021).